Soft Matter

Role of the supracellular actomyosin cable during epithelial wound healing

Journal:	*Soft Matter*
Manuscript ID	SM-ART-12-2017-002521.R1
Article Type:	Paper
Date Submitted by the Author:	26-Apr-2018
Complete List of Authors:	Yang, Yanjun; Rice University, Applied Physics and Center for Theoretical Biological Physics Levine, Herbert; Rice University, Bioengineering and Center for Theoretical Biological Physics

Journal Name

ARTICLE TYPE

Cite this: DOI: 10.1039/xxxxxxxxxx

Role of the supracellular actomyosin cable during epithelial wound healing†

Yanjun Yang[a] and Herbert Levine[b]

Received Date
Accepted Date

DOI: 10.1039/xxxxxxxxxx

www.rsc.org/journalname

The closure of wounds in epithelia is center to many physiological processes in both development and repair of multicellular organisms. Depending on the biochemical and mechanical environment as well as cell type, this collective cellular movement often involves coordinated cell crawling and the purse-string contraction of a supracellular actomyosin ring around the wound. However, it remains uncertain how these two mechanisms cooperatively contribute to the wound healing, and especially the role of the ring is not clear. To decipher this complex process, we develop a particle-based model that includes purse-string contraction, cell crawling and other properties incorporated with monolayers of Madin-Darby canine kidney (MDCK) cells. Our model captures the traction force patterns under several different conditions in experiments. In addition to traction force pointing away from the wound on the leading edge, we observed patterns of traction force pointing towards the wound. We show this inward pointing force pattern is induced by the purse-string contraction. Our model also explains the effects of the purse-string ring and which parameters affect the relative efficiency of these two mechanisms.

1 Introduction

Epithelial wound healing is a fundamental physiological process in multicellular organisms. Wounds need to be closed to re-establish the integrity of the epithelium and the physiological functions of the tissue [1–5]. This process is a complex collective behavior involving two major mechanisms: coordinated cell crawling mediated by lamellipodial and filopodial protrusions [6–11] and purse-string contraction of a supracellular actomyosin ring surrounding the wound [11–14]. Usually, actomyosin contractility is an important regulator in collective cellular migrations [17].

Recent experiments have proposed several factors that regulate the wound closure mechanisms including substrate adhesion, wound size and geometry [11,13–15,28]. On adhesive substrates, the cell crawling mechanism seems to predpminantly drive the wound closure, especially for a large wound. In this situation, the wound boundary is usually rough during the closure process [16]. Sometimes leader cells with fingering-like structures are also observed on the leading edge. [6] On non-adhesive substrates where cells cannot crawl, the purse-string contraction of a supracellular actomyosin ring seems to become the crucial mechanism for the wound closure. [13,14] In this kind of cases, the wound edge is usually smooth and the shape of the wound will often become 'rounder' during this process [15,16]. The actomyosin cable behaves differently depending on the geometry of the wound. It pulls the concave edge forward while pulling the convex edge backward [15]. These two mechanisms are not mutually exclusive, instead, they often coexist and interplay with each other [11,15]. However, due to the intrinsic complexity of this collective cellular behavior, how these two mechanisms contribute to the wound closure has not been fully understood yet. It is never easy to separate these factors and study these mechanisms individually in experiment.

Wound healing has also been studied by mathematical modeling. Particle-based computational simulations are developed to describe collective cellular movements [27]. Simulations have shown that cell crawling alone is sufficient to close a wound. These particle-based model have successfully reproduced the major aspects of wound healing driven by cell crawling [18]. Meanwhile, a continuous model which "de-activates" the actin dynamics on the wound boundary also shows that the wound can be closed without the actomyosin cable. [26] Several other continuous models, which describe the tissue as a viscoelastic material and model the actomyosin ring as a cable under tension, can capture the purse-string mechanism phenomenologically but without any direct connection to the cellular level dynamics [13–15]. A different model based on a Voronoi tessellation did consider contributions from these two mechanisms but with somewhat arbitrary assumptions about the temporal dynamics of the ring [11]. In addition, these models involving a supracellular actomyosin ring are

[a] Department of Applied Physics and Center for Theoretical Biological Physics, Rice University, Houston TX, 77251-1892, USA. E-mail: yanjun.yang@rice.edu
[b] Department of Bioengineering and Center for Theoretical Biological Physics, Rice University, Houston TX, 77251-1892, USA. E-mail: herbert.levine@rice.edu
† Electronic Supplementary Information (ESI) available: [details of any supplementary information available should be included here]. See DOI: 10.1039/b000000x/

nevertheless specially designed to fit a specific experiment.

In this article, we develop a more advanced particle-based model to address those unexplained effects in this complex process, especially the role of the supracellular actomyosin ring. The starting point for this model is our recent work focused on explaining expanding and migrating sheets of monolayer Madin-Darby canine kidney (MDCK) cells[19]. We add to this framework a model of the supracellular actomyosin ring as a set of mechanical links connecting neighboring cells around the wound. These links will form a ring on the wound rim and the tension exerted on these links will simulate purse-string contraction of the actomyosin ring. In our model, each cell exerts traction force on the substrate. We successfully reproduce the force patterns and healing dynamics for wound closure on both adhesive and non-adhesive substrates from experiments. In addition, we discuss the interplay of these two mechanisms. Remarkably, we build a framework which can incorporate actomyosin cables in different situations through this example.

2 Key mechanisms in the model

We utilize a two-dimensional sub-cellular element approach in our simulation. Each cell is represented by two particles, the front and the rear particle. Each particle is self-propelled with a self-propulsion force m. This self-propulsion force balances the intracellular contraction f_{contr} between the front and the rear particle (Fig. 1a), and it is subjected to contact inhibition of locomotion (CIL), meaning the propulsion force is suppressed by cell-cell contact and it aligns away from its neighbors. (More details in Supporting Information)[19]. The force between particles from different cells $f_{rep/adh}$ is repulsive at short distances, attractive at longer distances and becomes zero further away, which models the volume exclusion and cell-cell adhesions. (Fig. 1b) We assumed an overdamped particle dynamics because of strong substrate adhesion and calculate the velocity for each particle by

$$v = \frac{1}{\xi}(m + f_{contr} + f_{rep/adh}),$$

where ξ is the friction coefficient between particles and the substrate. The position for each particle is updated by a simple Euler scheme $x = vdt$. The traction force exerted on each particle from the substrate is $m - \xi v$.

In our simulation, we assume cell proliferation based on size. Each cell divides at a given probability when it excels a certain threshold length[19]. At each simulation step, we check the length of each cell, if a cell is longer than the threshold length, it divides at a certain probability. Upon division, a new particle is inserted near each particles from the original cell, forming two new cells. We distinguish motile and non-motile cells in our model. For a motile cell, the front particle has a larger magnitude of the self-propulsion force (m_f) than the rear particle (m_r). A non-motile cell has a same magnitude of the self-propulsion force for both the front and the rear particle. We inherit an alignment of cellular motility from our earlier model, in which each cell tends to align its motility force with its average velocity by switching between motile and non-motile states[19,20]. The switch between motile and non-motile states provides the stochasticity in our model[19,20]. However, this alignment plays a relatively minor role on the mechanical effects in our simulation as compared with CIL[19].

To model the supracellular actomyosin cable around the wound, we distinguish 'boundary cells' around the wound boundary. Particles of these 'boundary cells' are mechanically linked with their neighbors by a contraction force f_{cable} behaving like the intracellular contraction f_{contr}. (Fig.1a) These connections of neighboring cells around the wound will eventually form a whole purse-string contraction ring, which models the supracellular actomyosin cable on the wound rim. In our simulation, we can control the cable density by changing the connecting rules, for example, changing the maximum allowed links for each particle. In addition to this cable, 'boundary cells' have a larger maximum cell-cell adhesion with each other and their neighboring regular cells. (Fig.1b) (More details in the Support Information.) We will show this stronger cell-cell adhesion is necessary to form the observed traction force patterns.

3 Results

3.1 Closure of a circular wound

Our model can simulate the closure of a circular wound and obtain traction force patterns. We initialize our simulation by setting a circular hard wall in the center of a box surrounded by hard walls and seeding the cells around the circular hard wall. Cells will proliferate and eventually reach a steady state. After that, we remove the circular hard wall and label the first 1-2 rows of cells around the wound as 'boundary cells'. Cells start to close the wound after the formation of the supracellular actomyosin cable around the wound. We redefine the 'boundary cells' at every step according to their positions to ensure the ring is on the wound boundary.

We observed that cells are moving towards the wound center uniformly during the closure process in our simulation. (Supplementary movie S1.) The velocity for most cells are pointing to the wound center. We compute the average radial velocity as a function of distance from the wound center for every recorded moment during the process. The resulted average velocity is represented by a spatiotemporal kymograph (Fig. 2f). We show that the highest velocity emerges on the wound boundary (Fig. 2i) and there is also a time evolution of the velocity for each row of cells (Fig. 2f).

Our model can provide us the traction force for each particle at every time step (Fig. 2a-2c). We calculate the average radial (T_r) and scalar tangential ($|T_t|$) traction force components as a function of distance from the wound center and represent them in spatiotemporal kymographs. A clear spatiotemporal pattern is shown in the resulting kymographs (Fig. 2d, 2e). The radial traction force for the first row of cells is pointing away from the wound during the whole closure process. Immediate after the first row, there is a second layer where the radial traction force is pointing towards the wound (Fig. 2d). The traction force is not purely radial at the wound boundary. The kymograph of the average scalar tangential traction force shows a significant tangential component of the traction force on the wound boundary

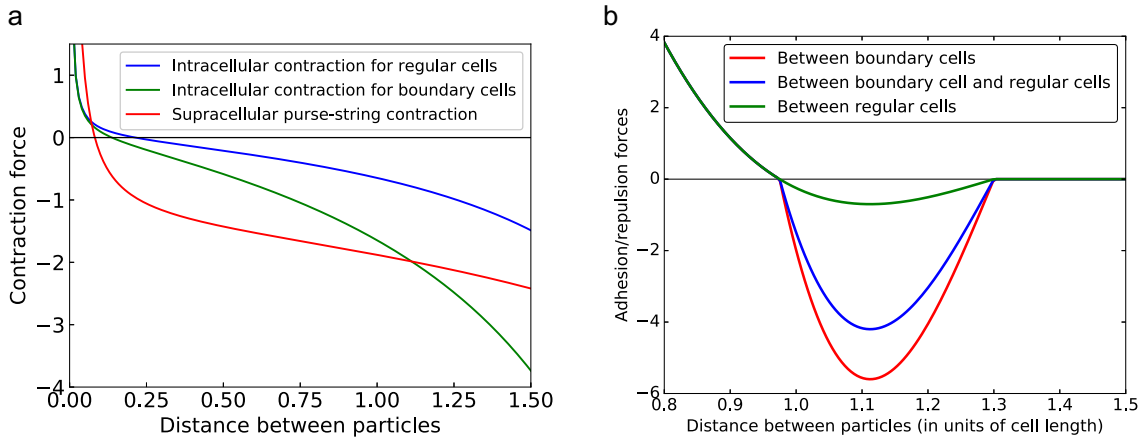

Fig. 1 Particle forces in model simulation. a. Contraction force. **b.** Intercellular adhesion/repulsion force.

(Fig. 2e). This comes from the heterogeneity of the actomyosin cable. Experiments reveal similar kymographs with an outward-pointing traction layer (OPTL) on the wound boundary and an inward-pointing traction layer (IPTL) immediate behind it, for example in experiments by Brugués et al. (Fig. 2j) [11]. The OPTL is related to the cell crawling, which has been observed many times in expanding tissues [10,21]. The IPTL is associated with the supracellular actomyosin cable. It originates from the interplay of the purse-string contraction of the ring, the intracellular cytoskeletal contraction and the cell-cell adhesions. Ultimately, It is a result of force transmission of the ring contraction to the substrate.

In the absence of the supracellular actomyosin ring, the wound can be closed by cell crawling alone and the absence of the ring does not affect the closure efficiency in general [32]. We observe that the closure time under these conditions are in a similar range (Fig. 2k). In both cases, wound area exhibits an approximate exponential decay, which is similar to behaviors observed during the contraction phase in Abreu-Blanco et al.'s experiments [16]. For wound closure dominated by cell crawling, we notice the wound edge is usually rougher as observed in experiments [32]. More importantly, the traction force patterns are substantially different. In absence of the ring, the OPTL will span much further behind the wound edge and the IPTL will not emerge, which indicates that cell crawling dominates the wound closure process (Fig. 3). Similar kymographs were also obtained by Brugues et al. from experiments [11]. Note that inward-pointing traction does eventually emerge, but only after the wound is fully closed. This is because that cells stop crawling after the closure but the pressure still remains. Without the ring, the wound edge becomes more rough and the cells exhibit more heterogeneity in their movements as is reflected by the tangential components of the traction force (Fig. 3e). Cell-cell adhesion and intracellular cytoskeletal contraction are also essential in this collective behavior. Either weaker intracellular cytoskeletal contraction or cell-cell adhesions between 'boundary cells' will impair or even destroy the IPTL; this is shown in Supporting Information (Fig. S2). The force transmission and the formation of the ring will be suppressed. The cell crawling is more favorable in this situation.

3.2 Closure of a circular wound on non-adhesive substrate

The purse-string from the supracellular actomyosin ring combined with the intracellular cytoskeletal contraction and the cell-cell adhesions is sufficient to close a small non-adhesive wound where cells cannot crawl [13,14]. In our simulation, we initialize this simulation in the same way as for the closure of a regular adhesive wound, except that we create a non-adhesive region in the center of the wound on which the cells cannot crawl. Once cells enter this non-adhesive circle their self-propulsion force m will be set to zero. In this non-adhesive region, the collective migration of cells towards the wound center is solely driven by the purse-string of the ring. In absence of the ring, cells will move around instead of towards the non-adhesive region [19,22] .

In our simulation, small wounds can be closed by this supracellular actomyosin ring, which agrees with experiments [13,14]. (Supplementary movie S2.) For large wounds, however, cells can only proceed into the non-adhesive region for about one-cell length. These cells are 'suspended' over the non-adhesive region by actin cables and cell-cell junctions [13,14]. Only in cases of sufficiently small wounds, can cells form a continuous structure bridging over the non-adhesive region and anchor on the non-adhesive boundary via focal adhesions. This kind of collective behavior is necessary for the closure of a non-adhesive wound. Recent experiments also observed that monolayer epithelia cells can bridge and suspend over distances while remain functional [23,24]. We again can compute spatiotemporal kymographs for the tractions (Fig. 4a-4c). The resulting kymographs show the largest traction is exerted on the non-adhesive edge (Fig. 4d-4e). We can also see that the average traction force as a function of distance to the wound center at a given time also reaches its maximum near the non-adhesive boundary (Fig. 4f-4g). These findings suggest a force transmission from the purse-string contraction to the cells at the edge of the non-adhesive region. This force transmission is reflected by the traction force exerted on the cells at the non-adhesive boundary.

The closure of wounds on non-adhesive substrate usually take a significantly longer time with large fluctuations. We recorded the dynamics of ten simulated wound closures with a non-adhesive region at the center of the wound. Once the frontier cells en-

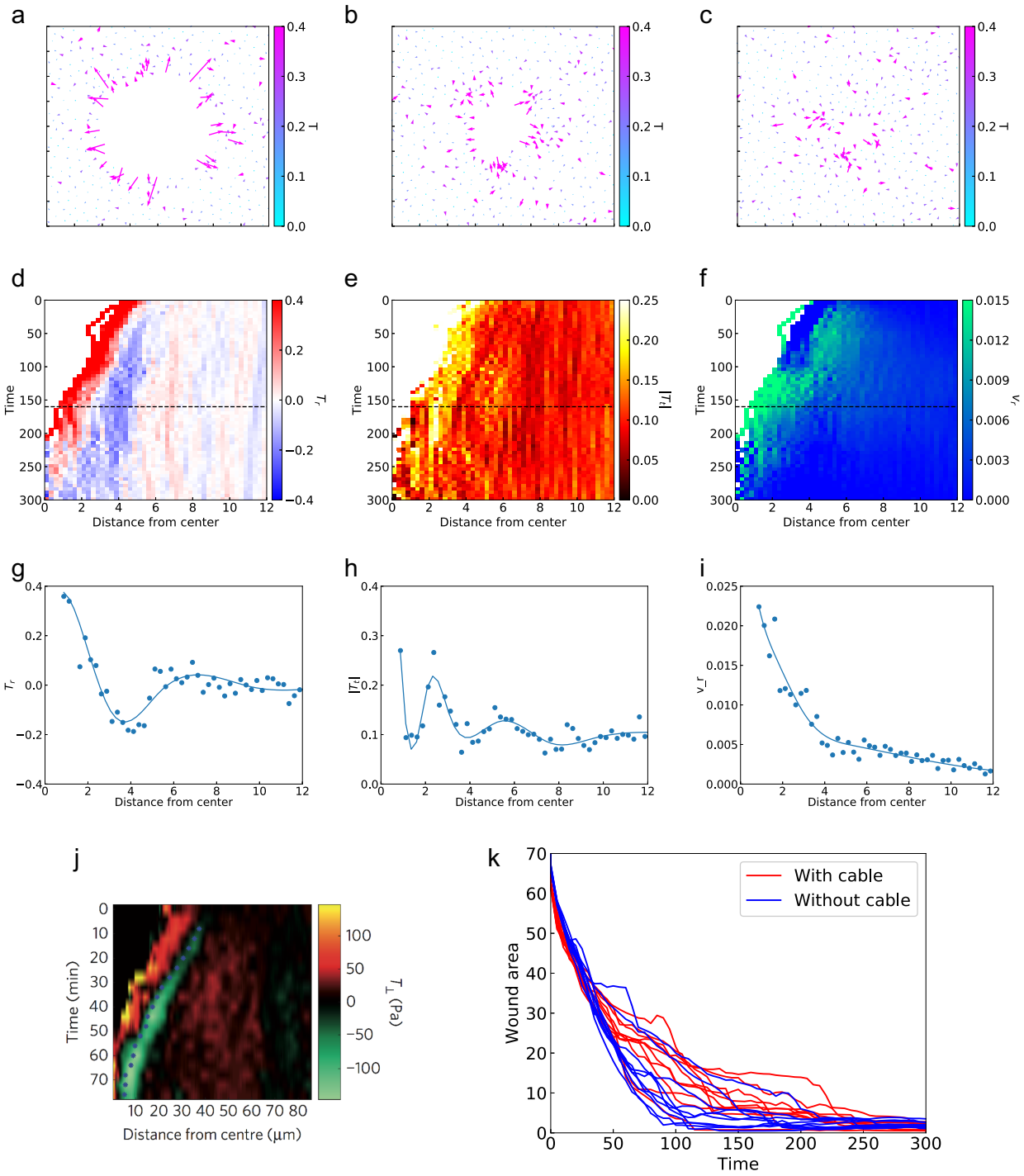

Fig. 2 Traction forces and wound healing dynamics for wounds on an adhesive substrate. a-c. Traction force patterns at three different time points: t=20, t=120 and t=200; color is based on the magnitude, and positive forces point away from the wound center. **d.** Kymograph for the radial component of traction force T_r. **e.** Kymograph for the tangential component of traction force $|T_t|$. **f.** Kymograph for the radial component of the cell velocity v_r. **g.** T_r across the horizontal dashed line in **d. h.** $|T_t|$ across the horizontal dashed line in **e. i.** v_r across the horizontal dashed line in **f.** The solid lines in **g-i** are merely guides to the data. **j.** Kymograph for T_r from experiment in ref.[11]. **k.** Dynamics of wound healing on an adhesive substrate. Parameters are the same as in Table S1. All units are simulation units.

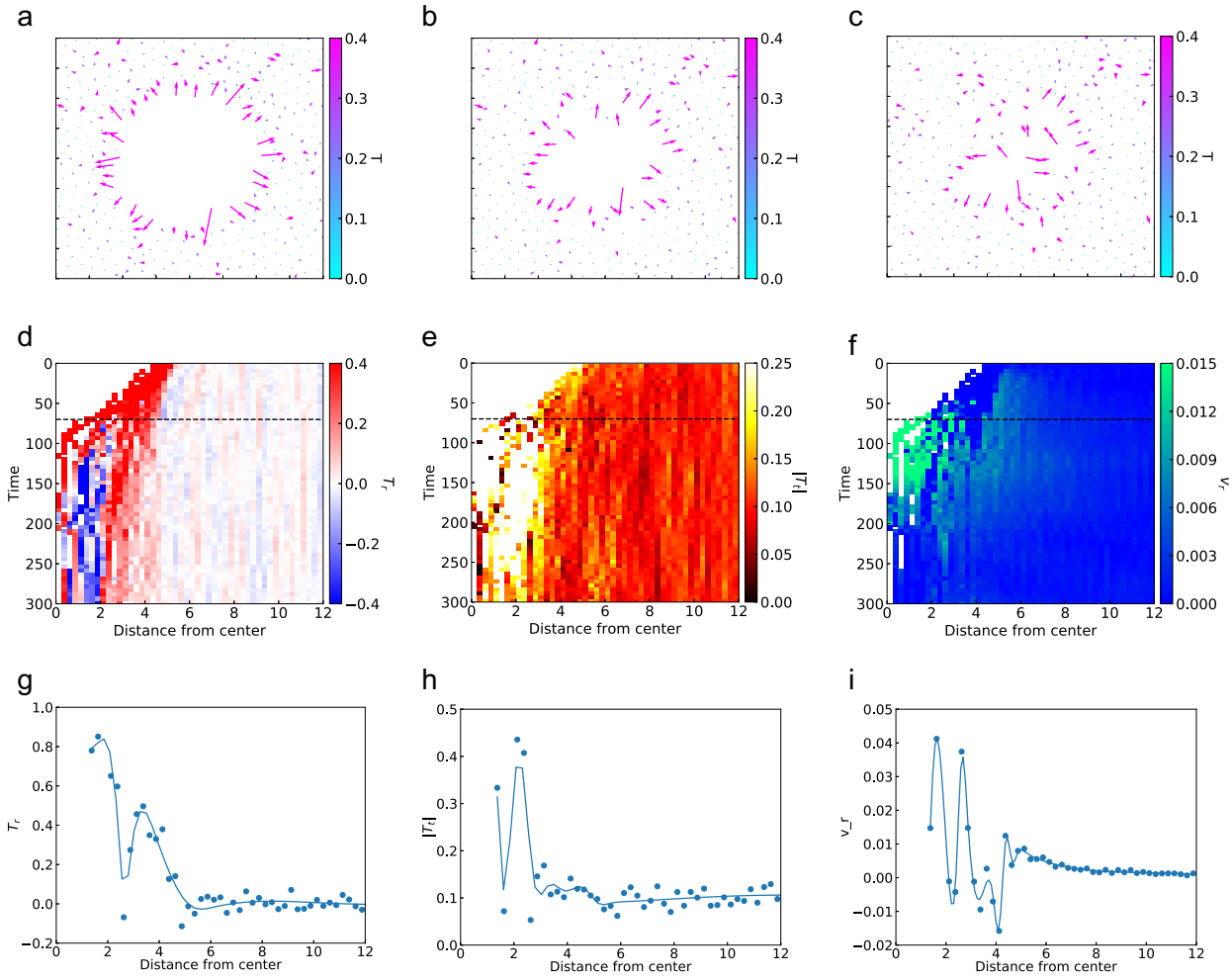

Fig. 3 Traction forces in absence of the actomyosin ring for wounds on an adhesive substrate. a-c. Traction force patterns at three different time points: t=20, t=60 and t=100; color is based on the magnitude, and positive forces point away from the wound center. **d.** Kymograph for the radial component of traction force T_r. **e.** Kymograph for the tangential component of traction force $|T_t|$. **f.** Kymograph for the radial component of the cell velocity v_r. **g.** T_r across the horizontal dashed line in **d**. **h.** $|T_t|$ across the horizontal dashed line in **e**. **i.** v_r across the horizontal dashed line in **f**. The solid lines in **g-i** are merely guides to the data. The width of the 'boundary cell' region $d = 0$, and other parameters are the same as in Table S1. All units are simulation units.

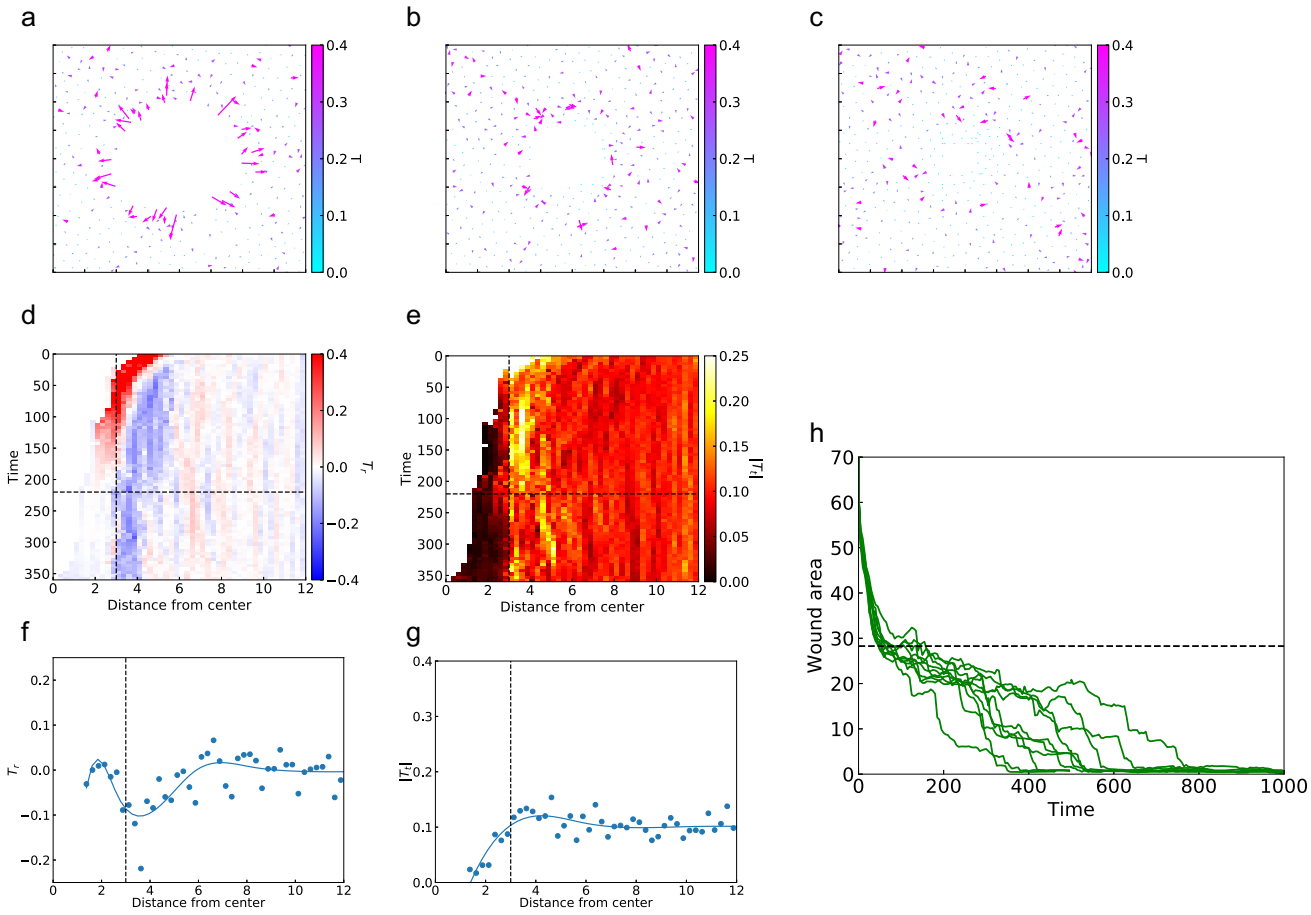

Fig. 4 Traction forces and wound healing dynamics for wounds on a non-adhesive substrate. a-c. Traction force patterns at three different time points: t=20, t=180 and t=340; color is based on the magnitude, and positive forces point away from the wound center. **d.** Kymograph for the radial component of traction force T_r. **e.** Kymograph for the tangential component of traction force $|T_t|$. **f.** T_r across the horizontal dashed line in **d**. **g.** $|T_t|$ across the horizontal dashed line in **e**. The solid lines in **f-g** are merely guides to the data. The vertical dashed lines in **d-g** indicate the non-adhesive boundary. **h.** Dynamics of wounds healing on non-adhesive substrate. The horizontal dashed line in **h** indicates the non-adhesive boundary. The radius of the non-adhesive region $R_{non-adh} = 3.0$, self-propulsion force $m_{f/r}$ are set to zero when particles enter the non-adhesive region, and other parameters are the same as in Table S1. All units are simulation units.

ter the non-adhesive region (horizontal dashed line in Fig. 4h), the closure rate drops, and cells move gradually towards the center of the wound with the sole drive from the actomyosin cable. There are two stages after the cells enter the non-adhesive region: the wound shrinks at a low rate for a long time with large fluctuations; then the wound closes rapidly. Similar dynamics were reported from experiments [13,14]; the slowly closing first stage corresponds to the growing period of the actomyosin cable. Because of this stage, the closure of a non-adhesive region can be up to 10 times slower than the closure of an adhesive region with the same area. Note the radius of the non-adhesive region is smaller than the wound, we are comparing the closure time for wound region with same size of the non-adhesive region.

3.3 Wound geometry

In our simulation, we also initialized wounds with geometries containing both convex and concave regions. Our model shows that wound geometry affects the efficiency of the supracellular actomyosin cable. The actomyosin cable will promote cellular movement at concave regions while hindering cell crawling at convex regions [15]. In our simulation, the largest traction force lies on tip of the convex region and points away from the wound. Such force pattern indicates a strong cell crawling suppressed by the actomyosin cable. On concave regions, however, the purse-string contraction of the ring pulls cells inwards the wound (Fig.5). Our simulation also shows that at convex edges cells are moving at a slower pace than cells at concave edges.

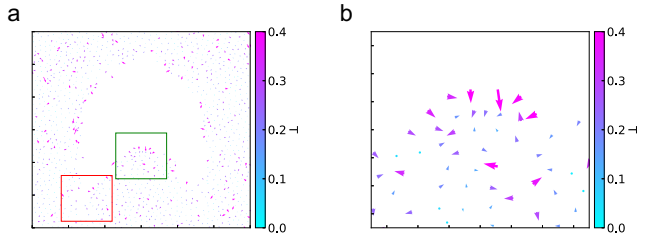

Fig. 5 Traction force at different curvatures. a. Overall traction force pattern. **b.** Zoomed-in view of the Green box as an example of a convex region. 'Boundary cells' are decided in a different way as discussed in Supporting Information, all parameters except circular wound related parameters, which are not applicable here, are the same as in Table S1. All units are simulation units.

3.4 Interplay between cell crawling and the actomyosin ring

As already discussed, these two mechanisms usually coexist although it is often sufficient to close a wound with only one of them. However, the purse-string mechanism of the actomyosin ring is unstable on adhesive surfaces. It is often observed that fast cellular movements suppress the efficiency and even the formation of the supracellular actomyosin cable [8]. In general, therefore, a tissue requires a sufficiently strong actomyosin cable to cooperate with the cell crawling. Otherwise, the cell crawling will dominate the wound closure process. In fact, Fenteany et al. provides several situations where the cell crawling dominates the wound healing [32]. In our simulation, if we reduce the number of mechanical links between boundary cells, we find the OPTL expands and the IPTL becomes weaker or even disappears (Fig.6a). The density of the actomyosin ring (the average number of links on wound rim) also drops at early times during the closure process (Fig.6d red line). In our model, CIL promotes the movements of cells on the wound edge. We can tune the strength of cellular movements by adjusting the level of CIL for the boundary cells (more details in Supporting Information [19]). We find that for lower level of CIL, we need fewer mechanical connections (compared with simulations with original level of CIL and cell crawling) between boundary cells to form an efficient actomyosin ring that is sufficient to induce a more obvious IPTL on the traction force pattern (Fig.6b). In this case, no initial drop of the actomyosin ring density is observed (Fig.6d green line). A comparison of the density of actomyosin rings in these two simulations and the simulation in Fig.2 is shown in Fig.6d.

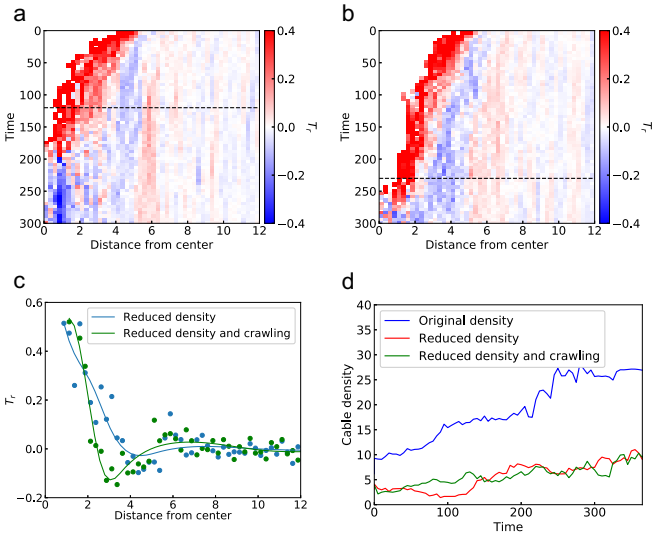

Fig. 6 Traction force for a relatively weaker actomyosin ring. a. Kymograph for T_r from a simulation with a weaker actomyosin ring and a same level of cell crawling as before. **b.** Kymograph for T_r from a simulation with the same level of weaker actomyosin ring but with a weaker cell crawling as well. **c.** T_r across the horizontal dashed line in **a-b**. The solid lines are merely guides to the data. **d.** Density of the actomyosin rings (average number of links on wound boundary). Blue line for simulation in figure 2, red line for simulation in **a**, and green line for simulation in **b**. In these two simulations, only front particles of 'boundary cells' can connect to each other when forming the supracellular actomyosin cable, the level of CIL $c_{inh} = 2.0$ for figure b, and other parameters are the same as in Table S1. All units are simulation units.

4 Discussion and conclusions

We have performed simulations for wound closure of cellular monolayer on a substrate and explored the combined effects of cell crawling and purse-string actomyosin. In our model, the supracellular actomyosin cable is formed by a intercellular mechanical links which are taken to be similar to the force modeling intracellular contraction. We assumed both intracellular and intercellular cables a similar origin and in fact, the wound rim also has a high concentration of actin and myosin that are found in intracellular contractive cables [11,15]. Similar supracel-

lular actomyosin cables were also found on sides of leader cell-guided finger-like protrusions on the leading edge of migrating cell colonies[6,25]. Thus, supracellular actomyosin cables are common and have an important mechanical role in collective cellular migration. Investigating the role of the supracellular actomyosin cable in other scenarios, especially in the finger-like protrusions, will be the subject of future work.

Past work on particle-based models which incorporate some aspects of a supracellular actomyosin cable on the border of expanding tissues have addressed several possible roles of such a cable[29]. However, such models have not previously been applied to the healing of a circular wound, meaning they have not been tested in this scenario. For wound closure, particle-based models have only considered cell crawling[18]. There has also been work on using continuous models as a method to introduce a supracellular actomyosin cable for these scenarios. Here, the interaction between cells is often described as a viscous interaction and the purse-string contraction was modeled as a cable under tension in continuous models. Vedula et al. assumed a cable tension increase linearly with local curvature to fit their experiment[14]. Ravasio et al. applied a similar model for to explain the relative contributions of the cable and cell crawling in their experiment and addressed how the wound geometry affects the efficiency[15]. Nier et al. used a stochastic model to describe the wound closure dynamics[13]. However, most of these models are very phenomenological and are typically designed for one specific experiment. A Voronoi tessellation based model introduced by Brugues et al. could capture the force patterns in their experimental data but required a time-dependent purse-string force which increases in strength with time in order to fit the experiment (Reference[11] Supplementary Information).

Recently, vertex models have been used to characterize the jamming transition in tissue[30,31]. This type of model could be applied in other situations. Specifically, the supracellular actomyosin cable can be easily included in a vertex model by applying additional tension on the wound edge.

Our model captures the key features in a relatively simple manner. Our simulation for wound healing under different conditions exhibits good agreement with experiments, especially in term of the traction force patterns[11,14,15]. We show that the purse-string mechanism due to the supracellular actomyosin ring determines the IPTL on kymographs of the traction force. This mechanism is the only drive available for wounds closure on non-adhesive substrates. On the other hand, these two mechanisms often coexist and interact with each other on adhesive substrates. Our model suggests that fast moving cells will suppress the efficiency of the actomyosin ring, while this ring will also hinder the cell advancement at convex regions. Only at concave regions will the actomyosin ring enhance the cell crawling.

In addition to the force patterns, our simulation also reproduces the dynamics in different experiments[13,14]. We show that the existence of the actomyosin cable has only a slight influence on the closure time of a wound on adhesive substrate. In this case, the actomyosin cable does not accelerate the wound closure though such structure is often observed. Meanwhile, for wounds on non-adhesive substrate, there is a slowly healing phase which corresponds to the growth of the cable. This period often lasts a long time, which makes the closure of a wound on non-adhesive substrate up to 10 times slower than a same size wound on an adhesive substrate. The stochasticity in our model is sufficient to capture these fluctuations.

In our current model, we mainly focus on the consequence of this actinmyosin cable and our approach is sufficient for that purpose. The ability to correctly account for cable effects in this example of wound healing gives us confidence that the same idea can be applied more generally. To make further progress, we will need a better understanding of the formation process of the supracellular actomyosin cable. We expect that the formation of the supracellular actomyosin cable is regulated by many different factors such as biochemical and mechanical cues, geometry of the wound etc. All these regulators can also affect the mechanical properties of the supracellular actomyosin cable via changing the density and strength of actin, myosin etc. The cellular-level remains to be fully understood.

Conflicts of interest

In accordance with our policy on Conflicts of interest please ensure that a conflicts of interest statement is included in your manuscript here. Please note that this statement is required for all submitted manuscripts. If no conflicts exist, please state that "There are no conflicts to declare".

Acknowledgements

This work was supported by the National Science Foundation Center for Theoretical Biological Physics (NSF PHY-1427654), and NSF DMS-1361411.

References

1 P. Martin, Wound healing– Aiming for perfect skin regeneration, Science, 1997, 276, 75-81.

2 T. J. Shaw and P. Martin, Wound repair at a glace, J. Cell Sci., 2009, 122, 3209-3213.

3 T. Lecuit and P. F. Lenne, Cell surface mechanics and the control of cell shape, tissue patterns and morphogenesis, Nat. Rev. Mol. Cell Biol., 2007, 8: 633-644.

4 K. J. Sonnemann and W. M. Bement, Wound repair: toward understanding and integration of single-cell and multicellular wound responses, Annu. Rev. Cell Dev. Biol., 2011, 27, 237-263.

5 S. Begnaud et al., Mechanics of epithelial tissues during gap closure, Curr. Opinion in Cell Biol., 2016, 42, 52-62.

6 M. Reffay et al., Interplay of RhoA and mechanical forces in collective cell migration driven by leader cells, Nat. Cell Biol., 2014, 16, 217-223.

7 M. Poujade et al., Collective migration of an epithelial monolayer in response to a model wound, Proc. Natl. Acad. Sci. USA, 2007, 104, 15988-15993.

8 O. Cochet-Escartin et al., Border Forces and Friction Control Epithelial Closure Dynamics, Biophys J., 2014, 106, 65-73.

9 E. Anon et al., Cell crawling mediates collective cell migration

to close undamaged epithelial gaps, Proc. Natl. Acad. Sci. USA, 2012, 109, 10891-10896.

10 X. Trepat et al., Physical forces during collective cell migration, Nat. Phys., 2009, 5, 426-430.

11 A. Brugues et al., Forces driving epithelial wound healing, Nat. Phys., 2014, 10, 683-690.

12 M. Tamada et al., Two distinct modes of myosin assembly and dynamics during epithelial wound closure, J. Cell Biol., 2007, 176, 27-33.

13 V. Nier et al., Tissue fusion over nonadhering surfaces, Proc. Natl. Acad. Sci. USA, 2015, 112, 9546-9551.

14 S. R. K. Vedula et al., Mechanics of epithelial closure over non-adherent environments, Nat. Comm., 2015, 6, 6111.

15 A. Ravasio et al., Gap geometry dictates epithelial closure efficiency, Nat. Comm., 2015, 6, 7683.

16 M. T. Abreu-Blanco et al., Drosophila embryos close epithelial wounds using a combination of cellular protrusions and an actomyosin purse string, J. Cell Sci., 2012, 125, 5984-5997.

17 A. J. Loza et al., Cell density and actomyosin contractility control the organization of migrating collectives within an epithelium, Mol. Biol. of the Cell, 2016, 27, 3459-3470

18 D. S. Li, J. Zimmermann, H. Levine, Modeling closure of circular wounds through coordinated collective motion, Phys. Biol., 2016, 13, 016006.

19 J. Zimmermann, B. A. Camley, W.-J. Rappel, H. Levine, Contact inhibition of locomotion determines cell-cell and cell-substrate forces in tissues, Proc. Natl. Acad. Sci. USA, 2016, 113, 2660-2665.

20 M. Basan, J. Elgeti, E. Hannezo, W.-J. Rappel, H. Levine, Alignment of cellular motility forces with tissue flow as a mechanism for efficient wound healing, Proc. Natl. Acad. Sci. USA, 2013, 110, 2452-2459.

21 O. D. Roure et al., Force mapping in epithelial cell migration, Proc. Natl. Acad. Sci. USA, 2005, 102, 2930-2395.

22 J. H. Kim et al., Propulsion and navigation within the advancing monolayer sheet, Nat. Mat., 2013, 12, 856-863.

23 S. R. K. Vedula et al., Epithelial bridges maintain tissue integrity during collective cell migration, Nat. Mat., 2014, 13, 87-96.

24 A. R. Harris et al., Characterizing the mechanics of cultured cell monolayers, Proc. Natl. Acad. Sci. USA, 2012, 109, 16449-16454.

25 B. Ladoux, R.-M. Mege, X. Trepat, Front-Rear Polarization by Mechanical Cues: From Single Cells to Tissues, Trends in Cell Biol., 2016, 26, 420-433.

26 P. Lee, C. W. Wolgemuth, Crawling Cells Can Close Wounds without Purse Strings or Signaling, PLoS Comput. Biol. 2011, 7, e1002007.

27 N. Sepulveda et al., Collective Cell Motion in an Epithelial Sheet Can Be Quantitatively Described by a Stochastic Interacting Particle Model, PLoS Comput. Biol. 2013, 9, e1002944.

28 G. C. Gurtner, S. Werner, Y. Barrandon and M. T. Longaker, Wound repair and regeneration, Nature, 2008, 453, 314-321.

29 V. Tarle, A. Ravasio, V. Hakim and N. S. Gov, Modeling the finger instability in an expanding cell monolayer, Integr. Biol., 2015, 7, 1218-1227.

30 D. Bi, J. H. Lopez, J. M. Schwarz and M. L. Manning, A density-independent rigidity transition in biological tissues, Nat. Phys. 2015, 11, 1074-1080.

31 D. Bi, X. Yang, M. C. Marchetti and M. L. Manning, Motility-driven glass and jamming transitions in biological tissues, Phys. Rev. X, 2016, 6, 021011.

32 G. Fenteany, P. A. Janmey and T. P. Stossel, Signaling pathways and cell mechanics involved in wound closure by epithelial cell sheets, Curr. Biol. 2000, 10, 831-838.

We demonstrate how the supracellular actomyosin cable contribute to the epithelial wound healing and its interplay with other mechanisms.